

# A new magnitude–redshift relation based on Type Ia supernovae

Ósmar Rodríguez<sup>1,2,\*</sup> and Alejandro Clocchiatti<sup>1,2</sup>

<sup>1</sup> Pontificia Universidad Católica de Chile, Vicuña Mackenna 4860, Macul, Santiago, Chile

<sup>2</sup> Instituto Milenio de Astrofísica (MAS), Nuncio Monseñor Sótero Sanz 100, Of. 104, Santiago, Chile

Received X; accepted Y

## ABSTRACT

We present a new empirical relation between the standardized magnitude ( $m$ ) of Type Ia supernovae (SNe Ia) and redshift ( $z$ ). Using Pantheon+ and DES-SN5YR, we find a negative linear correlation between  $m - 5 \log(z(1+z))$  and  $z$ , implying that their magnitude–redshift relation can be parametrized with just two parameters: an intercept  $\mathcal{M}$  and a slope  $b$ . This relation corresponds to the luminosity distance  $d_L(z) = c H_0^{-1} z(1+z) 10^{b z/5}$  and is valid up to at least  $z \simeq 1.1$ . It outperforms the  $\Lambda$ CDM and flat  $w$ CDM models and the (2,1) Padé approximant for  $d_L(z)$ , and performs comparably to the flat  $\Lambda$ CDM model and the (2,1) Padé ( $j_0 = 1$ ) model of Hu et al. Furthermore, the relation is relatively stable in the absence of low- $z$  SNe, making it suitable for fitting Hubble diagrams of SNe Ia without the need to add a low- $z$  sample. In deep fields in particular, assuming that the large-scale density is independent of the comoving radial coordinate,  $b \propto q_0 + 1$ . We fit the empirical relation to Hubble diagrams of eight deep-field regions, finding no evidence for anisotropy. The inferred  $q_0$  values, ranging from  $-0.6$  to  $-0.4$ , are consistent within  $1.6 \sigma$  and significantly lower than zero, indicating statistically consistent cosmic acceleration across all eight regions. We apply the empirical relation to the DES-Dovekie and Amalgame SN samples, finding  $b$  values consistent with those from DES-SN5YR and Pantheon+. Finally, using the empirical relation in the hemispheric comparison method applied to Pantheon+ up to  $z = 1.1$ , we find no evidence for anisotropies in  $\mathcal{M}$  and  $b$ .

**Key words.** supernovae: general – cosmological parameters – cosmology: theory

## 1. Introduction

General Relativity and the assumption of homogeneity and isotropy of the Universe at large scales are two of the foundations of modern cosmology. The latter leads to the Friedmann–Lemaître–Robertson–Walker (FLRW) metric, under which Einstein’s field equations reduce to the Friedmann equations. The first, combined with the FLRW metric, provides a formula for the luminosity distance–redshift relation,  $d_L(z)$ , in terms of three parameters: the Hubble constant ( $H_0$ ), the matter density ( $\Omega_M$ ), and the cosmological constant ( $\Lambda$ ) with density parameter  $\Omega_\Lambda$ .

Using Hubble diagrams of Type Ia supernovae (SNe Ia), Riess et al. (1998) and Perlmutter et al. (1999) found  $\Omega_\Lambda > 0$  and a deceleration parameter  $q_0 < 0$ , indicating that the expansion of the Universe is currently accelerating. In this context,  $\Lambda$  is interpreted as a scalar related to a hypothetical dark energy that drives cosmic acceleration. Given that models with  $\Lambda$ , when fitted to various observational data, yield  $\Omega_\Lambda > 0$  (Weinberg et al. 2013), the existence of dark energy has been widely accepted, consolidating the  $\Lambda$ CDM model as the standard model.

Despite its ability to fit observations, the  $\Lambda$ CDM model has problems of fine-tuning, cosmic coincidence, and tensions in cosmological parameters measured with independent experiments (Perivolaropoulos & Skara 2022; Efstathiou 2025). These issues have motivated alternative gravitational theories to explain cosmic acceleration without  $\Lambda$  (Koyama 2016; Odintsov et al. 2025). Moreover, cosmic acceleration may be partly an apparent effect associated with the assumption of homogeneity and isotropy and the corresponding use of the FLRW metric (Räsänen 2006; Enqvist 2008; Wiltshire 2009).

Cosmography provides a model-independent framework to study cosmic acceleration, expressing  $d_L(z)$  in terms of spatial curvature and kinematic parameters, such as  $H_0$ ,  $q_0$ , and the jerk parameter ( $j_0$ ). This approach, however, relies on the assumption of a homogeneous and isotropic Universe (Hu & Wang 2022).

Among current SN Ia samples, such as Pantheon+ (Brout et al. 2022) and DES-SN5YR (Sánchez et al. 2024), a significant fraction of the SNe originates from deep-field surveys. Analyzing deep fields separately allows one to infer direction-dependent parameters, without requiring global homogeneity and isotropy. In particular, comparing deep fields across different directions provides a test of isotropy.

Since angular variations in deep fields are expected to be negligible, and assuming that the large-scale density within each field is independent of the comoving radial coordinate, the metric can be approximated as FLRW on a field-by-field basis. Under this assumption, it might be possible to measure  $q_0$  for each deep field using the FLRW metric, without assuming global homogeneity and isotropy. The main limitation of this approach is the small number of low- $z$  SNe Ia ( $z < 0.1$ ) in deep fields, which are crucial for breaking parameter degeneracies (Linder 2006).

One approach to reducing the impact of the lack of low- $z$  SNe on the estimation of  $q_0$  is to use a  $d_L(z)$  relation with as few parameters as possible. In the flat  $\Lambda$ CDM model,  $d_L(z)$  depends only on  $H_0$  and  $\Omega_M$ . The latter, which is used to measure  $q_0$ , remains relatively stable in the absence of low- $z$  SNe (Brout et al. 2022). To date, the only other  $d_L(z)$  relation that accurately fits SN observations with just two parameters is the one proposed by Hu et al. (2024a). It corresponds to a third-order Padé approximation with  $H_0$  and  $q_0$  as free parameters, while  $j_0$  is fixed to one, as predicted by the flat  $\Lambda$ CDM model (Bochner et al. 2015).

\* Corresponding author: olrodrig@gmail.com

In this work, we introduce an empirical magnitude–redshift relation ( $m(z)$ ) and the corresponding  $d_L(z)$  relation, which provides a straightforward quantitative tool to fit Hubble diagrams of SNe Ia up to at least  $z \simeq 1.1$ , using only two parameters and without assuming any theoretical model or spatial curvature. This relation is relatively stable in the absence of low- $z$  SNe, making it suitable for studying SN deep fields without the need to add a low- $z$  sample.

The paper is organized as follows. In Sect. 2, we describe the SN samples and define the deep-field regions. In Sect. 3, we present the  $m(z)$  relations employed to fit Hubble diagrams. In Sect. 4, we present the results, including the new empirical relation, its comparison with five  $m(z)$  relations, and its application to the deep-field regions and to other samples. In Sect. 5, we discuss the derived  $j_0$  values, the search for cosmic anisotropies, and future analyses. Our conclusions are summarized in Sect. 6.

## 2. Data samples

Pantheon+<sup>1</sup> contains data from 1550 SNe Ia, drawn from 18 surveys, with  $0.001 \leq z \leq 2.261$ . DES-SN5YR<sup>2</sup> contains data from 1635 photometrically classified SNe Ia from the DES-SN program with  $0.060 \leq z \leq 1.121$ , and 194 SNe Ia from four surveys, with  $0.025 < z < 0.093$ , referred to as the low- $z$  sample.

Pantheon+ and DES-SN5YR provide RA and Dec coordinates; standardized SN magnitudes ( $m_B^{\text{corr}}$ , hereafter  $m$ ), derived from SALT2 (Pantheon+) and SALT3 (DES-SN5YR) light-curve fits, and corrected for stretch, color, host-galaxy mass, and selection bias; redshifts corrected for the CMB dipole and peculiar velocities ( $z_{\text{HD}}$ , hereafter  $z$ ); and the covariance matrix ( $\mathbf{C}$ ) to account for statistical and systematic errors.

As done by Brout et al. (2022), from Pantheon+ we select SNe with  $z > 0.01$  to minimize the impact of peculiar velocities on the derived cosmological parameters. In the following, we refer to this subsample simply as Pantheon+. Because DES-SN5YR introduced several improvements compared to Pantheon+, their  $m$  values are not on the same scale. In particular, there is a constant offset of 0.04 mag between selection bias corrections in DES-SN5YR and Pantheon+, which does not impact the cosmological results from each separate analysis (Vincenzi et al. 2025). Hence, we analyze both samples separately.

Fig. 1 shows the sky distribution of the SNe in Pantheon+ and DES-SN5YR. SNe with  $z \geq 0.4$  are concentrated in small regions of the sky, which reflects the location of the SN deep fields. We define 14 circular regions for Pantheon+ and four for DES-SN5YR, referred to as XY, which contain virtually all SNe with  $z \geq 0.4$ . In this notation, X denotes the closest Galactic pole and Y indicates the rank of proximity to that pole. Table 1 lists the regions, their centers in (RA, Dec), angular radii ( $\theta$ ), number of SNe within each region, and the corresponding  $z$  ranges.

The S1, S2, S4, and S5 regions in Pantheon+ closely match those in DES-SN5YR. In these regions, DES-SN5YR contains 170–490 more SNe than Pantheon+, while 47–100% of the SNe in the Pantheon+ S1, S2, S4, and S5 regions come from the DES-SN program and are already included in DES-SN5YR. Therefore, we use only DES-SN5YR data for these regions.

The remaining ten Pantheon+ regions contain 13–77 SNe each. To increase the sample while minimizing sky area, we define the triangular N147, N235, and S367 regions. N147 includes N1, N4, N7, and the SNe located within the triangle formed by

**Table 1.** SN regions

Region	RA (°)	Dec (°)	$\theta$ (°)	$z$ range	#SNe
Pantheon+					
S1	8.57	−43.36	1.60	0.148–0.609	34
S2	35.56	−4.88	2.12	0.017–1.912	134
S3	352.15	−0.09	2.17	0.079–0.508	34
S4	41.89	−0.21	2.19	0.134–0.638	57
S5	53.78	−28.00	1.89	0.103–1.549	97
S6	333.83	−17.70	0.61	0.371–0.789	44
S7	333.68	0.20	2.14	0.040–0.419	43
N1	185.14	47.10	1.37	0.025–0.545	24
N2	213.64	53.01	1.47	0.082–1.615	64
N3	189.24	62.22	0.10	0.840–2.261	13
N4	162.85	58.30	1.52	0.023–0.503	20
N5	242.82	54.96	1.40	0.122–0.576	30
N6	150.05	2.18	1.51	0.047–1.543	77
N7	130.55	44.39	1.44	0.071–0.578	37
S367	339.96	−5.10	–	0.015–0.789	163
N147	158.83	52.31	–	0.023–0.578	89
N235	216.91	58.56	–	0.082–2.261	107
DES-SN5YR					
S1	8.63	−43.53	1.76	0.073–0.818	295
S2	35.57	−5.32	2.11	0.138–1.044	518
S4	42.00	−0.51	1.83	0.094–0.733	231
S5	53.83	−28.09	2.11	0.060–1.121	591

their centers; similarly for N235 and S367. For S367, we increase the declination of the centers of S3 and S7 by  $1.2^\circ$  to include more SNe without significantly increasing the area. The triangular regions are shown in Fig. 1, while their barycenters,  $N$ , and  $z$  ranges are listed in Table 1. We refer to the S1, S2, S4, S5, N147, N235, S367, and N6 regions as the deep-field regions.

## 3. Methods

### 3.1. Magnitude–redshift relations

The  $m(z)$  relation for a standard candle with absolute magnitude  $M$  is given by

$$m(z) = M + 5 \log \mathcal{D}_L(z), \quad (1)$$

where  $M = M + 5 \log(c H_0^{-1} \text{Mpc}^{-1}) + 25$  and  $\mathcal{D}_L(z) = d_L(z)H_0/c$ . To derive  $d_L(z)$  using either a gravitational theory or a cosmographic expansion, one needs the metric of the expanding Universe. The simplest choice is the FLRW metric, characterized by the scale factor  $a$  and the curvature parameter  $k$ . For this metric,

$$d_L(z) = (1+z)d_M(z), \quad (2)$$

where  $d_M(z)$  is the transverse comoving distance. Defining  $H(z) = \dot{a}/a$  and  $\Omega_k = -kc^2/H_0^2$ ,  $d_M(z)$  is given by

$$d_M(z) = \frac{c}{H_0} \begin{cases} \Omega_k^{-1/2} \sinh(\Omega_k^{1/2} \int_0^z \frac{H_0}{H(z')} dz') & \Omega_k > 0 \\ \int_0^z \frac{H_0}{H(z')} dz' & \Omega_k = 0 \\ |\Omega_k|^{-1/2} \sin(|\Omega_k|^{1/2} \int_0^z \frac{H_0}{H(z')} dz') & \Omega_k < 0 \end{cases}. \quad (3)$$

#### 3.1.1. $\Lambda$ CDM, flat $\Lambda$ CDM, and flat $w$ CDM models

In the phenomenological generalization of the  $\Lambda$ CDM model,

$$H(z) = H_0 \sqrt{\Omega_M(1+z)^3 + \Omega_k(1+z)^2 + \Omega_\Lambda(1+z)^{3(1+w)}}, \quad (4)$$

<sup>1</sup> <https://github.com/PantheonPlusSH0ES/DataRelease>

<sup>2</sup> <https://doi.org/10.5281/zenodo.12720778>

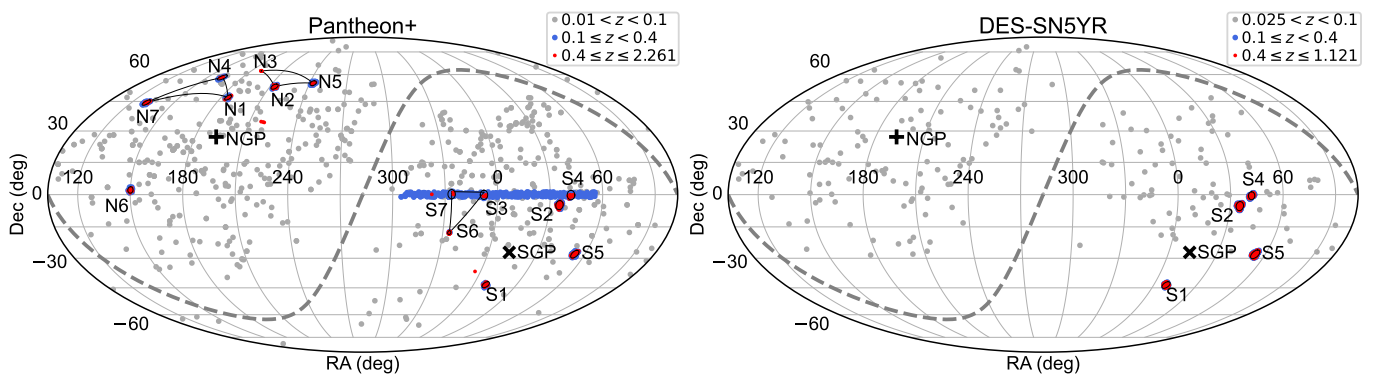


**Fig. 1.** Sky distribution of Pantheon+ and DES-SN5YR SNe. Dashed lines indicate the Galactic equator. Plus (cross) symbols mark the north (south) Galactic pole. Circular and triangular regions are also shown.

where  $\Omega_M + \Omega_\Lambda + \Omega_k = 1$  and  $w$  is the dark energy equation-of-state parameter. We use the  $m(z)$  relations for  $\Lambda$ CDM ( $w = -1$ ), flat  $\Lambda$ CDM ( $\Omega_k = 0$ ,  $w = -1$ ), and the phenomenological flat  $w$ CDM ( $\Omega_k = 0$ ) models.

### 3.1.2. Padé cosmography and flat Padé model

The Padé approximation is a method to approximate a function  $F(z)$  as the ratio of two polynomials of orders  $A$  and  $B$ . The rational function is known as the  $(A, B)$  Padé approximant, and its coefficients are expressed in terms of those of the Taylor series of  $F(z)$  truncated at order  $A + B$  (Baker & Graves-Morris 1996).

Hu & Wang (2022), using Pantheon (Scolnic et al. 2018), found that the  $(2, 1)$  Padé approximant for  $d_L(z)$  performs better than cosmographic expansions based on Taylor series. More recently, Hu et al. (2024a) analyzed Pantheon+ and found that this approximant outperforms other Padé forms. We therefore adopt it as the best cosmographic approach.

The  $(2, 1)$  Padé approximant for  $d_L(z)$  used by Hu et al. (2024a) was derived by Capozziello et al. (2020) for  $\Omega_k = 0$ . To compute the expression valid for any  $\Omega_k$ , we use the third-order Taylor series for  $d_L(z)$  (Eq. 2 of Cattoën & Visser 2007) and the procedure of Baker & Graves-Morris (1996), obtaining

$$d_L(z) = \frac{cz}{H_0} \frac{6(1 - q_0) + (5 - 8q_0 - 3q_0^2 + 2\hat{j}_0)z}{6(1 - q_0) + 2(1 - q_0 - 3q_0^2 + \hat{j}_0)z}. \quad (5)$$

Here,  $\hat{j}_0 \equiv j_0 - \Omega_k$ , and

$$q_0 = \left. \frac{d \ln H(z)}{dz} \right|_{z=0} - 1, \quad j_0 = \left. \frac{d^2 H(z)}{dz^2} \right|_{z=0} + q_0^2. \quad (6)$$

For  $\Omega_k = 0$ , Eq. (5) is equivalent to that given in Hu et al. (2024a). We refer to Eq. (5) as the Padé cosmography.

Hu et al. (2024a) also found that the  $(2, 1)$  Padé approximant for  $d_L(z)$  with  $j_0 = 1$  fixed performs better than the Padé cosmography, the flat  $\Lambda$ CDM,  $\Lambda$ CDM, and flat  $w$ CDM models. Since  $j_0$  was fixed to unity because this is the value for the flat  $\Lambda$ CDM model, the  $d_L(z)$  equation proposed by Hu et al. (2024a) is not cosmographic, but rather model-based. We refer to Eq. (5) assuming  $\hat{j}_0 = 1$  as the flat Padé model.

### 3.1.3. Empirical approach

To fit the Hubble diagram, we introduce the ansatz

$$d_L(z) = \frac{cz}{H_0} (1 + z) 10^{f(z)/5}, \quad (7)$$

where the factor  $1 + z$  is inspired by Eq. (2) and  $f(z)$  is a free function that vanishes as  $z \rightarrow 0$ , ensuring  $d_L(z) = cz/H_0$  at low  $z$ . The corresponding  $m(z)$  relation is

$$m(z) = \mathcal{M} + 5 \log(z(1 + z)) + f(z), \quad (8)$$

where the dependence of  $f(z)$  on  $z$  can be determined empirically from the correlation between  $m - 5 \log(z(1 + z))$  and  $z$ .

### 3.2. Parameter estimation and model selection

Let  $\mathbf{v}$  be the vector with the  $n_p$  free parameters of  $m(z)$ . The posterior probability of  $m(z)$  is  $P \propto p(\mathbf{v}) \mathcal{L}$ , where  $p(\mathbf{v})$  is the prior and  $\mathcal{L} = e^{-\chi^2/2}$ . Following Conley et al. (2011),

$$\chi^2 = \Delta \mathbf{m}^T \mathbf{C}^{-1} \Delta \mathbf{m}, \quad (9)$$

where  $\Delta \mathbf{m}$  is the vector of residuals, whose  $i$ -th component is

$$\Delta m_i = m_i - m(z_i, \mathbf{v}). \quad (10)$$

We assume uninformative priors; in this case, the best-fit parameter vector  $\mathbf{v}_{\text{best}}$  that maximizes  $P$  is obtained by minimizing  $\chi^2$ .

To calculate uncertainties, we use EMCEE (Foreman-Mackey et al. 2013), which samples  $P$  using a Markov Chain Monte Carlo (MCMC) process. First, we define the priors as flat distributions:  $\mathcal{M} \in (23, 25)$ ,  $\Omega_M \in (0, 1)$ ,  $\Omega_\Lambda \in (0, 1)$ ,  $w \in (-2, 0)$ ,  $q_0 \in (-2, 1)$ , and  $\hat{j}_0 \in (-4, 7)$ . These priors are wide enough to consider them as uninformative. Next, we initialize  $10n_p$  walkers in a tiny Gaussian ball around  $\mathbf{v}_{\text{best}}$  and run  $10^5$  steps ( $10^6$  for the flat  $w$ CDM model). Then, given an integrated autocorrelation time ( $\tau$ ) provided by EMCEE, we discard the initial  $3\tau$  steps as burn-in and thin by  $\tau/2$ . With this configuration, we obtain for all parameters a Gelman & Rubin (1992) statistic of  $\hat{R} \approx 1.0$ , indicating convergence of the MCMC chains, and an effective sample size  $n_{\text{eff}} > 2000$  ( $n_{\text{eff}} > 400$  for the flat  $w$ CDM model). Finally, for each parameter, we adopt the 68.27% confidence interval of its marginalized distribution as the  $1\sigma$  uncertainty.

To identify which model of a set of candidates best describes the Hubble diagram, we use the corrected Akaike information criterion (AICc; Sugiura 1978) and the Bayesian information criterion (BIC; Schwarz 1978). For each model, we compute  $\text{AICc} = \chi_{\text{min}}^2 + 2n_p N / (N - n_p - 1)$  and  $\text{BIC} = \chi_{\text{min}}^2 + n_p \ln N$ , where  $\chi_{\text{min}}^2 = \chi^2(\mathbf{v}_{\text{best}})$  and  $N$  is the number of SNe. Based on IC (AICc or BIC), the preferred model is the one with the smallest IC value ( $\text{IC}_{\text{min}}$ ), and the strength of evidence for each model is given by  $\Delta_{\text{IC}} = \text{IC} - \text{IC}_{\text{min}}$ . Models with  $\Delta_{\text{AICc}} < 2$  and  $4 < \Delta_{\text{AICc}} < 7$  have substantial and considerably less support, respectively (Burnham

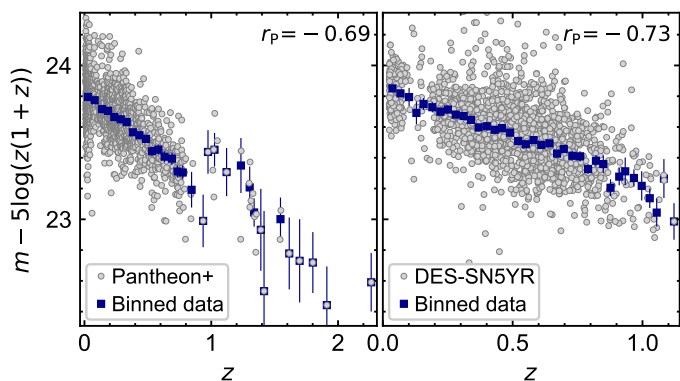


**Fig. 2.**  $m - 5 \log(z(1+z))$  versus  $z$  for Pantheon+ and DES-SN5YR. Binned data (blue squares) with error bars are shown for visualization purposes only, both here and throughout the paper.

& Anderson 2002), while  $\Delta_{\text{BIC}} < 2$  and  $6 < \Delta_{\text{BIC}} < 10$  indicate little and strong evidence against the model, respectively (Kass & Raftery 1995). Therefore, models with both  $\Delta_{\text{AICc}} < 2$  and  $\Delta_{\text{BIC}} < 2$  perform comparably, yielding comparable fits to the Hubble diagram, whereas models with larger  $\Delta_{\text{AICc}}$  or  $\Delta_{\text{BIC}}$  are increasingly less supported or disfavoured, respectively.

## 4. Results

### 4.1. Empirical relation

Fig. 2 shows  $m - 5 \log(z(1+z))$  versus  $z$  for Pantheon+ and DES-SN5YR. Their weighted Pearson correlation coefficients ( $r_p$ ; Earp et al. 2019) are close to  $-0.7$ , with  $p$ -values below  $10^{-220}$ , indicating a moderate-to-strong negative linear correlation. Based on this, we express  $m - 5 \log(z(1+z))$  as a linear function of  $z$ , with an intercept  $M$  and a slope  $b$ :

$$m(z) = M + bz + 5 \log(z(1+z)). \quad (11)$$

Thus,  $f(z) = bz$  in Eq. (8), and together with Eq. (7) yields

$$d_L(z) = \frac{cz}{H_0} (1+z) 10^{bz/5}. \quad (12)$$

We refer to Eqs. (11) and (12) as the empirical relation.

The empirical relation exhibits a series of characteristics. First, it is relatively stable to the absence of low- $z$  SNe (see Sect. 4.5). Second, its parameters and their associated covariance matrix can be computed analytically. Fig. 3 shows the confidence contours for  $M$  and  $b$  computed analytically and with EMCEE (using the flat prior  $b \in (-2, 0)$ ), which are virtually identical. Third, under the FLRW metric,  $b \propto q_0 + 1$ . Indeed, from Eqs. (12) and (2),

$$d_M(z) = \frac{cz}{H_0} 10^{bz/5}, \quad (13)$$

and using Eq. (16) of Li et al. (2020),

$$H(z) = H_0 \frac{\sqrt{10^{-2bz/5} + \Omega_k z^2}}{1 + b \ln(10)z/5} \quad (14)$$

which, together with Eq. (6), yields

$$q_0 = -\frac{2}{5} \ln(10)b - 1. \quad (15)$$

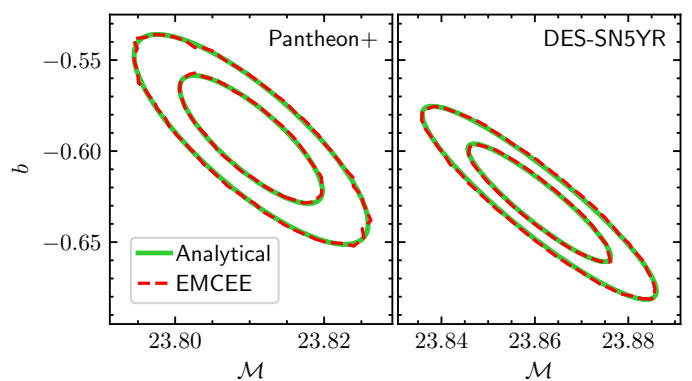


**Fig. 3.** Confidence contours at the 68.27% and 95.45% levels for the parameters of the empirical relation, obtained analytically and with EMCEE.

### 4.2. Constraints on cosmological parameters

Parameter constraints from Pantheon+ and DES-SN5YR for the six  $m(z)$  relations used in this work are listed in Table 2. The parameters for the flat  $\Lambda$ CDM,  $\Lambda$ CDM, and flat  $w$ CDM models are consistent with those reported by the Pantheon+ team ( $\Omega_M = 0.334 \pm 0.018$  for the flat  $\Lambda$ CDM model,  $\Omega_M = 0.306 \pm 0.057$  and  $\Omega_\Lambda = 0.625 \pm 0.084$  for the  $\Lambda$ CDM model, and  $\Omega_M = 0.309^{+0.063}_{-0.069}$  and  $w = -0.90 \pm 0.14$  for the flat  $w$ CDM model; Brout et al. 2022) and the DES Collaboration ( $\Omega_M = 0.352 \pm 0.017$  for the flat  $\Lambda$ CDM model,  $\Omega_M = 0.291^{+0.063}_{-0.065}$  and  $\Omega_\Lambda = 0.55 \pm 0.10$  for the  $\Lambda$ CDM model, and  $\Omega_M = 0.264^{+0.074}_{-0.096}$  and  $w = -0.80^{+0.14}_{-0.16}$  for the flat  $w$ CDM model; Camilleri et al. 2024).

For each  $m(z)$  relation, the parameters derived from DES-SN5YR and Pantheon+ are consistent within  $1\sigma$ , except for  $M$ , which shows differences greater than  $3.3\sigma$ . The discrepancy in  $M$  is due to the constant offset of 0.04 mag between selection bias corrections in DES-SN5YR and Pantheon+ (Vincenzi et al. 2025). Accounting for this offset, the  $M$  values derived from DES-SN5YR and Pantheon+ become consistent within  $1\sigma$ .

### 4.3. Hubble diagrams and model comparison

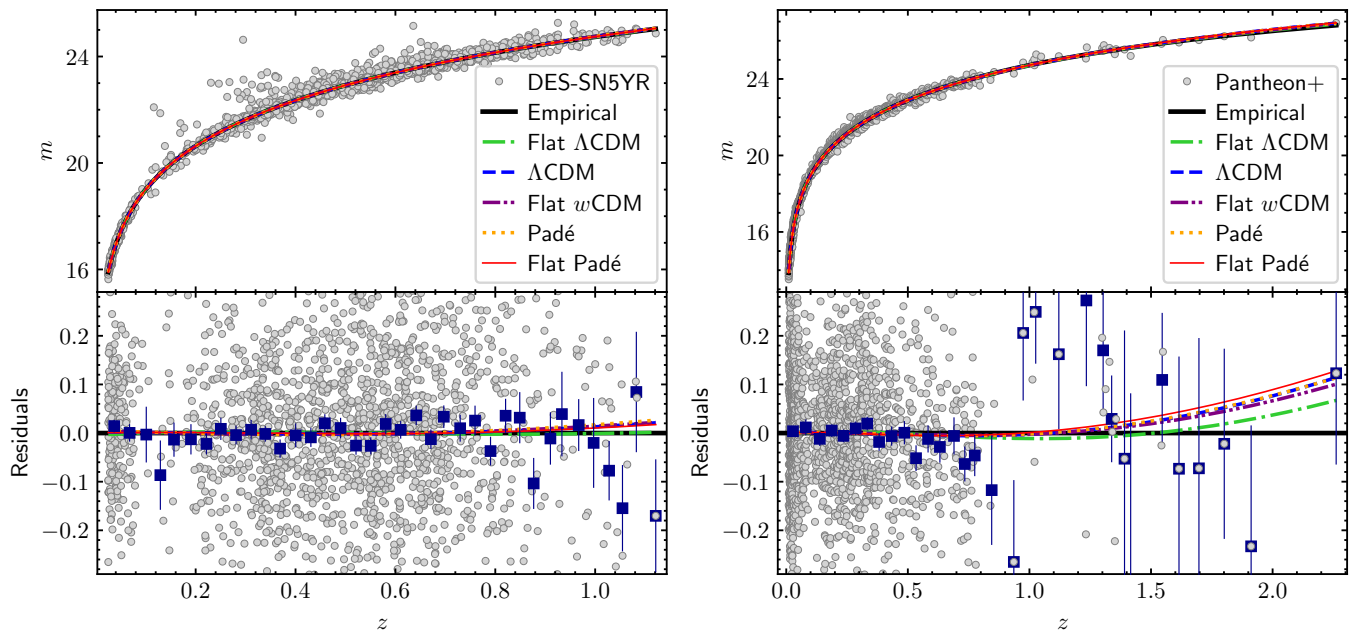
Fig. 4 shows the Hubble diagrams for DES-SN5YR and Pantheon+, the best fits for the  $m(z)$  relations, and the residuals relative to the empirical relation. For DES-SN5YR, the empirical relation provides a fit comparable to that of the other  $m(z)$  relations. The differences between the  $m(z)$  relations and the empirical relation have rms values below 0.009 mag and maximum absolute deviations  $\Delta m_{\text{max}}$  below 0.027 mag. For Pantheon+, the empirical relation starts to diverge from the other  $m(z)$  relations at  $z \gtrsim 1.4$ , and for  $z < 1.121$  (the highest  $z$  in DES-SN5YR), the rms and  $\Delta m_{\text{max}}$  remain below 0.007 and 0.012 mag, respectively.

Given that the empirical relation accurately reproduces the Hubble diagrams of both samples up to  $z = 1.121$ , we assume it is valid at least up to that redshift. Beyond it, its validity cannot be reliably assessed because Pantheon+ contains only 19 SNe at  $z > 1.121$ . In what follows, we restrict our analyses of Pantheon+, including its deep-field regions, to  $z < 1.121$ , although analyses without this cut lead to the same conclusions. Table 2 lists the parameter constraints for Pantheon+ ( $z < 1.121$ ).

Table 3 lists the  $\Delta_{\text{AICc}}$  and  $\Delta_{\text{BIC}}$  values. Based on these, the empirical relation, the flat  $\Lambda$ CDM model, and the flat Padé model provide comparable fits to the Hubble diagrams of DES-SN5YR and Pantheon+ ( $z < 1.121$ ), with the flat  $\Lambda$ CDM model being only marginally disfavoured for DES-SN5YR ( $\Delta_{\text{AICc}} = 2.2$  and  $\Delta_{\text{BIC}} = 2.1$ ). In contrast, the  $\Lambda$ CDM model, the flat  $w$ CDM

**Table 2.** Parameters constraints for different magnitude–redshift relations

Relation	$\mathcal{M}$	$b$	$\Omega_M$	$\Omega_\Lambda$	$w$	$q_0$	$\hat{f}_0$
DES-SN5YR							
Empirical	$23.861 \pm 0.010$	$-0.628 \pm 0.021$	–	–	–	–	–
Flat $\Lambda$ CDM	$23.857 \pm 0.011$	–	$0.350 \pm 0.017$	–	–	–	–
$\Lambda$ CDM	$23.863 \pm 0.013$	–	$0.297^{+0.060}_{-0.067}$	$0.566^{+0.093}_{-0.106}$	–	–	–
Flat $w$ CDM	$23.865 \pm 0.013$	–	$0.273^{+0.070}_{-0.101}$	–	$-0.82^{+0.16}_{-0.16}$	–	–
Padé	$23.866 \pm 0.014$	–	–	–	–	$-0.396^{+0.072}_{-0.112}$	$0.664^{+0.851}_{-0.452}$
Flat Padé	$23.861 \pm 0.011$	–	–	–	–	$-0.441 \pm 0.024$	–
Pantheon+							
Empirical	$23.810 \pm 0.006$	$-0.594 \pm 0.023$	–	–	–	–	–
Flat $\Lambda$ CDM	$23.807 \pm 0.007$	–	$0.331 \pm 0.018$	–	–	–	–
$\Lambda$ CDM	$23.810 \pm 0.008$	–	$0.298^{+0.053}_{-0.055}$	$0.619^{+0.077}_{-0.084}$	–	–	–
Flat $w$ CDM	$23.811 \pm 0.009$	–	$0.293^{+0.067}_{-0.073}$	–	$-0.91^{+0.14}_{-0.17}$	–	–
Padé	$23.809 \pm 0.010$	–	–	–	–	$-0.492^{+0.069}_{-0.111}$	$1.167^{+0.955}_{-0.502}$
Flat Padé	$23.811 \pm 0.007$	–	–	–	–	$-0.471 \pm 0.026$	–
Pantheon+ ( $z < 1.121$ )							
Empirical	$23.812 \pm 0.007$	$-0.606 \pm 0.026$	–	–	–	–	–
Flat $\Lambda$ CDM	$23.808 \pm 0.007$	–	$0.336 \pm 0.019$	–	–	–	–
$\Lambda$ CDM	$23.810 \pm 0.009$	–	$0.315^{+0.082}_{-0.091}$	$0.636^{+0.107}_{-0.121}$	–	–	–
Flat $w$ CDM	$23.809 \pm 0.010$	–	$0.324^{+0.074}_{-0.117}$	–	$-0.97^{+0.22}_{-0.21}$	–	–
Padé	$23.809 \pm 0.010$	–	–	–	–	$-0.505^{+0.082}_{-0.136}$	$1.323^{+1.324}_{-0.660}$
Flat Padé	$23.811 \pm 0.007$	–	–	–	–	$-0.468 \pm 0.028$	–


**Fig. 4.** DES-SN5YR and Pantheon+ Hubble diagrams, along with the best fits for the  $m(z)$  relations. The lower panels show the residuals relative to the empirical relation.

model, and the Padé cosmography are less supported by the AICc and disfavoured by the BIC, reflecting the penalty associated with their additional free parameter.

#### 4.4. Deceleration parameter and Hubble constant

Table 4 lists the  $q_0$  values. For the flat  $\Lambda$ CDM,  $\Lambda$ CDM, and flat  $w$ CDM models we use  $q_0 = \Omega_M/2 + (1 + 3w)\Omega_\Lambda/2$ . Although the empirical relation is developed only to fit Hubble diagrams, its  $q_0$  values are consistent with those of the other  $m(z)$  relations.

We estimate  $H_0$  using the empirical relation together with Pantheon+ ( $z < 1.121$ ) and the Cepheid distance moduli ( $\mu_{\text{Ceph}}$ )

from SH0ES (Riess et al. 2022). To do this, we replace Eq. (10) with  $\Delta m_i = m_i - M - \mu_{\text{Ceph},i}$  for those SNe hosted in galaxies with  $\mu_{\text{Ceph}}$ . We obtain  $M = -19.244 \pm 0.030$ ,  $b = -0.604 \pm 0.026$ , and  $H_0 = 73.4 \pm 1.0 \text{ km s}^{-1} \text{ Mpc}^{-1}$ . This  $H_0$  value is consistent with those obtained by Brout et al. (2022) from Pantheon+ and SH0ES, which range from  $73.3 \pm 1.1$  to  $73.6 \pm 1.1 \text{ km s}^{-1} \text{ Mpc}^{-1}$ .

#### 4.5. Stability in the absence of low- $z$ SNe

To evaluate the stability of the best-fit parameters of the six  $m(z)$  relations against the absence of low- $z$  SNe, we compute  $\mathcal{M}$  and  $q_0$  for different minimum redshifts ( $z_{\text{min}}$ ): 0.01, 0.03, 0.06, 0.10,

**Table 3.** AICc and BIC statistics

Relation	$\chi^2_{\min}$	AICc	BIC	$\Delta_{\text{AICc}}$	$\Delta_{\text{BIC}}$
DES-SN5YR					
Empirical	1638.1	1642.1	1653.2	0.0	0.0
Flat $\Lambda$ CDM	1640.3	1644.3	1655.3	2.2	2.1
$\Lambda$ CDM	1639.5	1645.5	1662.1	3.4	8.9
Flat $w$ CDM	1639.0	1645.0	1661.5	2.9	8.3
Padé	1639.4	1645.4	1662.0	3.3	8.8
Flat Padé	1639.7	1643.7	1654.7	1.6	1.5
Pantheon+ ( $z < 1.121$ )					
Empirical	1392.3	1396.3	1407.0	0.6	0.5
Flat $\Lambda$ CDM	1391.7	1395.7	1406.5	0.0	0.0
$\Lambda$ CDM	1391.7	1397.7	1413.7	2.0	7.2
Flat $w$ CDM	1391.7	1397.7	1413.8	2.0	7.3
Padé	1391.7	1397.7	1413.7	2.0	7.2
Flat Padé	1391.8	1395.8	1406.5	0.1	0.0

**Table 4.** Values of  $q_0$  for different magnitude–redshift relations

Relation	DES-SN5YR		Pantheon+ ( $z < 1.121$ )	
	$q_0$		$q_0$	
Empirical	$-0.422^{+0.019}_{-0.019}$		$-0.442^{+0.024}_{-0.024}$	
Flat $\Lambda$ CDM	$-0.475^{+0.026}_{-0.025}$		$-0.496^{+0.030}_{-0.028}$	
$\Lambda$ CDM	$-0.417^{+0.077}_{-0.067}$		$-0.478^{+0.081}_{-0.071}$	
Flat $w$ CDM	$-0.392^{+0.076}_{-0.074}$		$-0.483^{+0.096}_{-0.092}$	
Padé	$-0.396^{+0.072}_{-0.112}$		$-0.505^{+0.082}_{-0.136}$	
Flat Padé	$-0.441^{+0.025}_{-0.023}$		$-0.468^{+0.028}_{-0.027}$	

and 0.15. The resulting  $(M, q_0)$  points are shown in Fig. 5. We find that the empirical relation, the flat  $\Lambda$ CDM model, and the flat Padé model are the most stable in the absence of low- $z$  SNe. Since the best-fit parameters of the empirical relation are the intercept and slope of the approximately linear correlation between  $m - 5 \log(z(1+z))$  and  $z$  (see Fig. 2 and Eq. 11), their stability depends primarily on the  $z$  baseline of the data. Therefore, they are expected to vary only mildly when low- $z$  SNe are removed.

When fitted to DES-SN5YR, these three relations exhibit a gap between the cases with  $z_{\min} \geq 0.06$  and those with  $z_{\min} \leq 0.03$ . Since for  $z_{\min} \geq 0.06$  at least 85% of the SNe in the low- $z$  sample of DES-SN5YR are removed, one possible explanation is a difference between the  $m$  values of the low- $z$  sample relative to the rest of DES-SN5YR (Huang et al. 2025). This effect does not impact the analysis of the S1, S2, S4, and S5 deep-field regions, as they do not contain any SNe from the low- $z$  sample.

#### 4.6. Deep-field regions

Fig. 6 shows the Hubble diagrams for the deep-field regions. To constrain the parameters of the S1, S2, S4 and S5 regions, we select the  $m$  and  $z$  values for the SNe in these regions, along with the corresponding entries of the covariance matrix. Then, we replace Eq. (10) with  $\Delta m_i = m_i - m(z_i, \mathbf{v}_j)$  for those SNe within the  $j$ -th region with parameters  $\mathbf{v}_j$ . The same procedure is applied to the S367, N147, N235, and N6 regions. Table 5 lists the parameter constraints for the empirical relation and the flat  $\Lambda$ CDM and flat Padé models. The best fits are shown in Fig. 6.

Table 6 lists the  $\Delta_{\text{AICc}}$  and  $\Delta_{\text{BIC}}$  values for the empirical relation and the flat  $\Lambda$ CDM and flat Padé models. These values indicate that the three  $m(z)$  relations provide comparable fits to the Hubble diagrams in the deep-field regions. Since the empirical relation is purely phenomenological and its parameters,

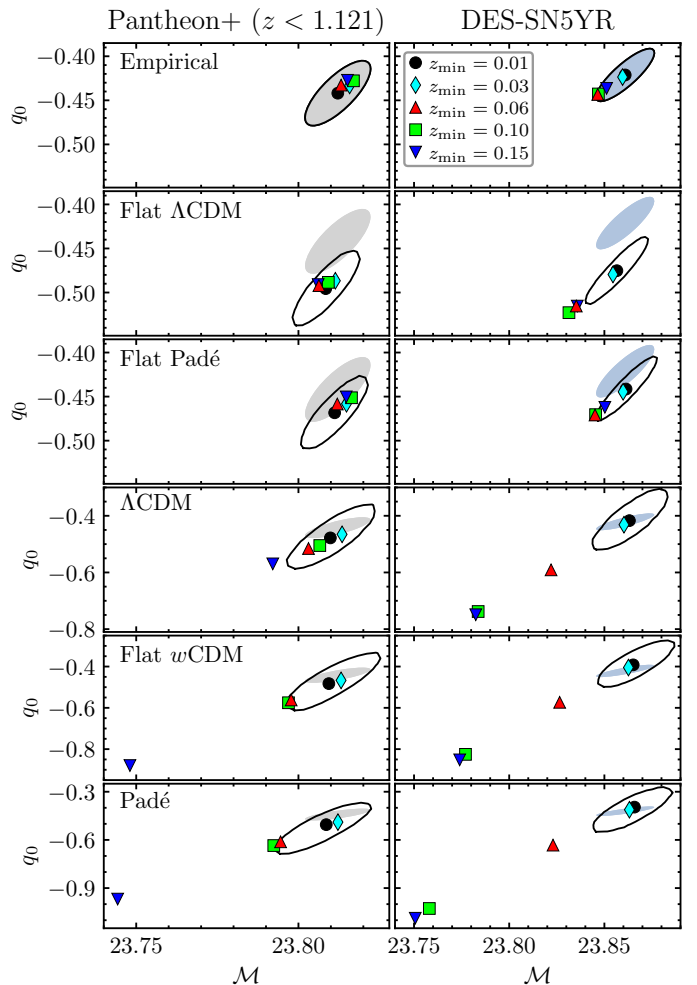


**Fig. 5.**  $q_0$  versus  $M$  for the  $m(z)$  relations fitted to DES-SN5YR and Pantheon+ ( $z < 1.121$ ) with different  $z_{\min}$ . Solid curves are the 68.27% confidence contours for  $z_{\min} = 0.01$ , while the contour of the empirical relation is shown as a shaded region in each panel for comparison. Note that, although the flat  $w$ CDM constraints in the  $(w, \Omega_M)$  plane are highly non-Gaussian, their projection onto  $q_0$  leads to nearly symmetric uncertainties, as expected since  $q_0 = Q_H(z=0)$ , where the parameter  $Q_H(z)$  is almost free of the  $w$ - $\Omega_M$  degeneracy (Camilleri et al. 2024).

uncertainties, and confidence contours can be computed analytically (Sect. 4.1), we use it as a convenient parametrization to characterize the deep-field regions.

Fig. 7 shows the confidence contours and the marginalized distributions for  $M$  and  $b$  for the deep-field regions. The  $b$  values are consistent within  $1.6\sigma$ . When accounting for the 0.04 mag offset between the selection bias corrections in DES-SN5YR and Pantheon+, the  $M$  values are consistent within  $1.6\sigma$ , in agreement with isotropy. Similar results are obtained when comparing the parameters of the flat  $\Lambda$ CDM and flat Padé models, where the differences in  $M$ ,  $\Omega_M$ , and  $q_0$  are no more than  $1.7\sigma$ ,  $1.5\sigma$  and  $1.7\sigma$ , respectively.

To test whether fitting the S1, S2, S4, and S5 regions with different parameters for each region (eight parameters in total) provides a significantly better fit than an isotropic fit (two parameters for all regions), we perform a likelihood ratio test (LRT). The test statistic  $\lambda = \chi^2_{\min, \text{iso}} - \chi^2_{\min}$ , where  $\chi^2_{\min}$  is the value for the model with eight parameters (listed in Table 6) and  $\chi^2_{\min, \text{iso}}$  is the value for the isotropic fit, follows a  $\chi^2$  distribution with six degrees of freedom (Wilks 1938). Fitting the empirical re-

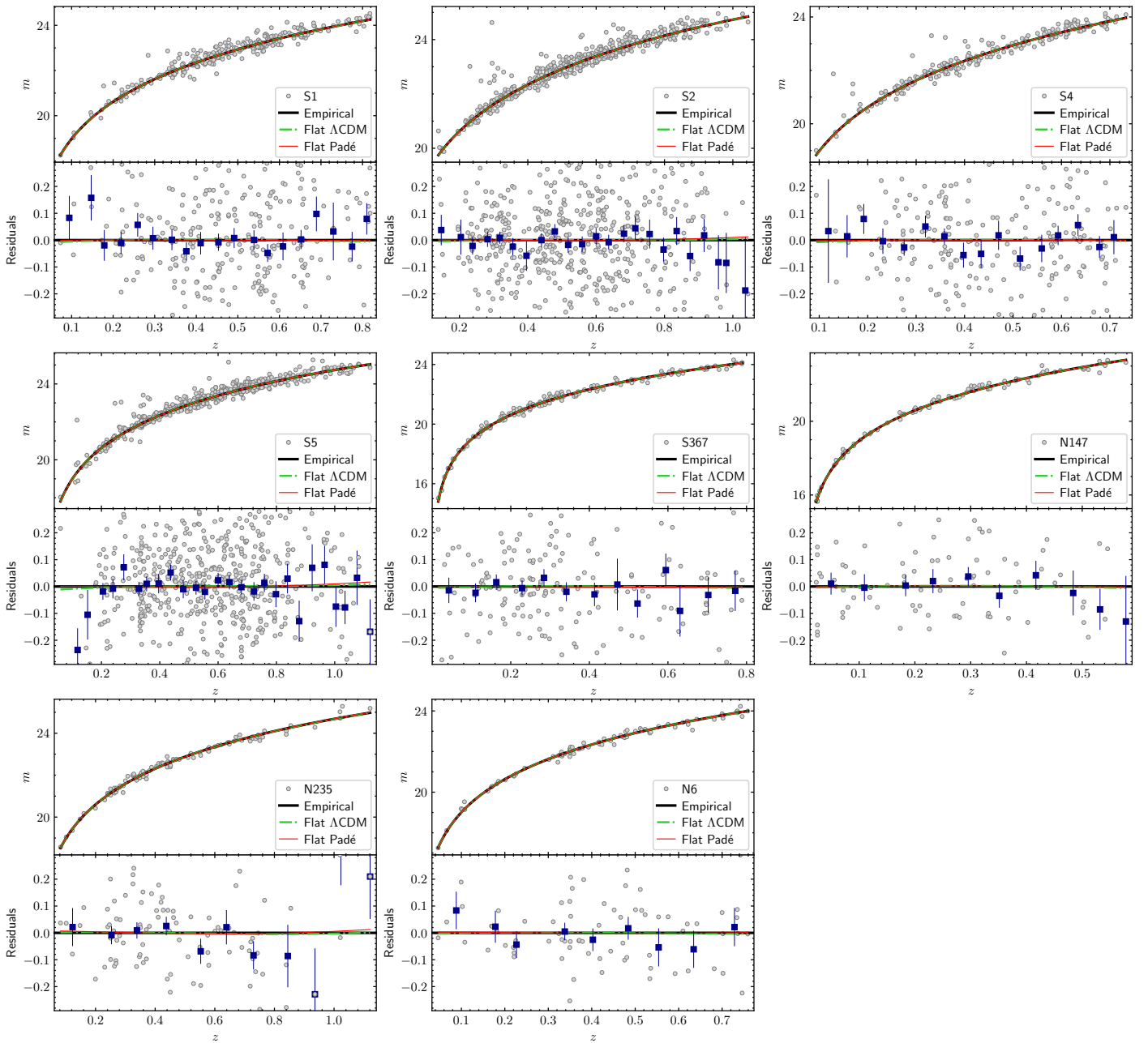


**Fig. 6.** Same as Fig. 4, but for the deep-field regions.

lation, we obtain  $\chi_{\min, \text{iso}}^2 = 1451.3$ ,  $\lambda = 8.4$ , and a  $p$ -value of 0.21. For the S367, N235, N147, and N6 regions, we obtain  $\chi_{\min, \text{iso}}^2 = 383.5$ ,  $\lambda = 6.7$ , and a  $p$ -value of 0.35. In both cases, the isotropic fit cannot be rejected. Similar results are obtained when using the flat  $\Lambda$ CDM and flat Padé models, where the LRT  $p$ -values are between 0.20 and 0.36. Therefore, we find no evidence for anisotropy in the Hubble diagrams of the deep-field regions.

Table 7 lists the  $q_0$  values for the deep-field regions. The values measured using the empirical relation are consistent within  $1.6\sigma$  and lower than zero by more than  $4.8\sigma$  (99.9998% confidence). These results indicate that the Universe is undergoing accelerated expansion in a statistically consistent manner across all eight deep-field regions, under the assumption that the large-scale densities in these regions are independent of the comoving radial coordinate.

## 4.7. Application to other samples

### 4.7.1. DES-Dovekie sample

While this work was nearing completion, a re-analysis of DES-SN5YR was presented by Popovic et al. (2025). The resulting recalibrated data set, DES-Dovekie,<sup>3</sup> includes an improved photometric cross-calibration and a fixed host-galaxy color law. Since DES-Dovekie supersedes DES-SN5YR (Popovic et al. 2025), its analysis provides the best constraints and overall results from DES-SN combined with a low- $z$  sample.

We fit the empirical relation ( $b = -0.603 \pm 0.020$ ), the Padé cosmography ( $q_0 = -0.444^{+0.072}_{-0.114}$ ,  $\hat{j}_0 = 0.805^{+0.881}_{-0.466}$ ), flat  $\Lambda$ CDM ( $\Omega_M = 0.329 \pm 0.015$ ),  $\Lambda$ CDM ( $\Omega_M = 0.286^{+0.056}_{-0.062}$ ,  $\Omega_\Lambda = 0.600^{+0.088}_{-0.102}$  or  $\Omega_k = 0.11^{+0.16}_{-0.14}$ ), flat  $w$ CDM ( $\Omega_M = 0.268^{+0.063}_{-0.086}$ ,  $w = -0.85 \pm 0.15$ ), and the flat Padé model ( $q_0 = -0.470 \pm 0.022$ ).

<sup>3</sup> <https://github.com/des-science/DES-SN5YR>

**Table 5.** Parameters constraints for the deep-field regions

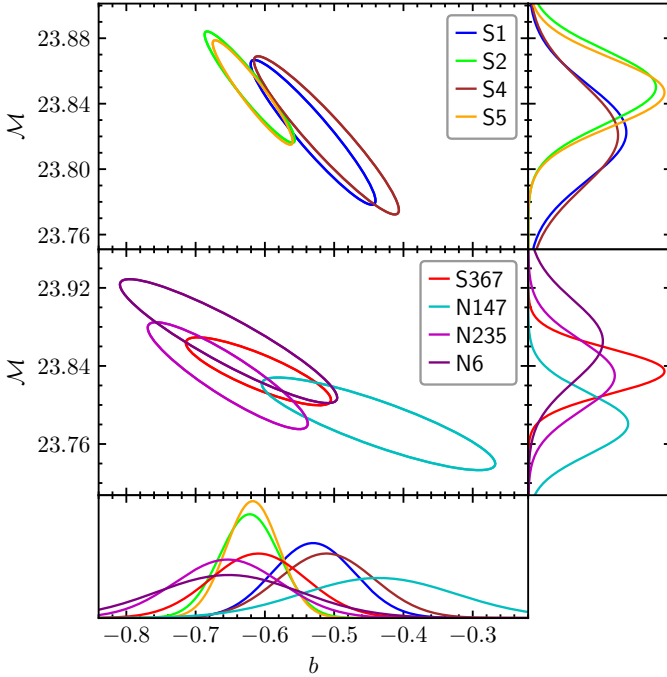
Region	Empirical relation		Flat $\Lambda$ CDM model		Flat Padé model	
	$M$	$b$	$M$	$\Omega_M$	$M$	$q_0$
S1	$23.823 \pm 0.029$	$-0.530 \pm 0.059$	$23.810^{+0.036}_{-0.028}$	$0.273^{+0.049}_{-0.037}$	$23.820^{+0.034}_{-0.028}$	$-0.548^{+0.070}_{-0.056}$
S2	$23.850 \pm 0.022$	$-0.622 \pm 0.043$	$23.837^{+0.029}_{-0.024}$	$0.333^{+0.042}_{-0.031}$	$23.851^{+0.027}_{-0.023}$	$-0.448^{+0.057}_{-0.047}$
S4	$23.821 \pm 0.032$	$-0.511 \pm 0.069$	$23.806^{+0.038}_{-0.030}$	$0.257^{+0.035}_{-0.040}$	$23.816^{+0.037}_{-0.031}$	$-0.571^{+0.079}_{-0.064}$
S5	$23.847 \pm 0.021$	$-0.618 \pm 0.038$	$23.831^{+0.027}_{-0.022}$	$0.327^{+0.036}_{-0.028}$	$23.846^{+0.025}_{-0.021}$	$-0.455^{+0.049}_{-0.041}$
S367	$23.834 \pm 0.023$	$-0.609 \pm 0.069$	$23.828^{+0.027}_{-0.022}$	$0.335^{+0.059}_{-0.045}$	$23.833^{+0.026}_{-0.022}$	$-0.465^{+0.083}_{-0.067}$
N147	$23.781 \pm 0.031$	$-0.436 \pm 0.111$	$23.775^{+0.035}_{-0.028}$	$0.227^{+0.078}_{-0.060}$	$23.778^{+0.034}_{-0.029}$	$-0.637^{+0.114}_{-0.092}$
N235	$23.830 \pm 0.036$	$-0.654 \pm 0.076$	$23.830^{+0.050}_{-0.038}$	$0.376^{+0.084}_{-0.056}$	$23.838^{+0.046}_{-0.037}$	$-0.397^{+0.111}_{-0.083}$
N6	$23.865 \pm 0.042$	$-0.652 \pm 0.103$	$23.862^{+0.055}_{-0.040}$	$0.370^{+0.103}_{-0.068}$	$23.868^{+0.051}_{-0.042}$	$-0.412^{+0.140}_{-0.103}$

**Table 6.** AICc and BIC statistics for the deep-field regions

Relation	$\chi^2_{\min}$	AICc	BIC	$\Delta_{\text{AICc}}$	$\Delta_{\text{BIC}}$
S367+N147+N235+N6					
Empirical	376.8	393.1	425.3	0.6	0.7
Flat $\Lambda$ CDM	376.2	392.5	424.7	0.0	0.1
Flat Padé	376.1	392.5	424.6	0.0	0.0
S1+S2+S4+S5					
Empirical	1442.9	1459.0	1502.1	0.0	0.0
Flat $\Lambda$ CDM	1443.9	1460.0	1503.1	1.0	1.0
Flat Padé	1444.6	1460.7	1503.8	1.7	1.7

**Table 7.** Values of  $q_0$  for the deep-field regions.

Region	$q_0$ (Empirical)	$q_0$ (Flat Padé)	$q_0$ (Flat $\Lambda$ CDM)
S1	$-0.511 \pm 0.055$	$-0.548^{+0.070}_{-0.056}$	$-0.591^{+0.075}_{-0.055}$
S2	$-0.427 \pm 0.040$	$-0.448^{+0.057}_{-0.047}$	$-0.500^{+0.062}_{-0.047}$
S4	$-0.529 \pm 0.064$	$-0.571^{+0.079}_{-0.064}$	$-0.615^{+0.083}_{-0.060}$
S5	$-0.431 \pm 0.035$	$-0.455^{+0.049}_{-0.041}$	$-0.510^{+0.055}_{-0.041}$
S367	$-0.439 \pm 0.064$	$-0.465^{+0.083}_{-0.067}$	$-0.497^{+0.089}_{-0.067}$
N147	$-0.598 \pm 0.102$	$-0.637^{+0.114}_{-0.092}$	$-0.660^{+0.117}_{-0.089}$
N235	$-0.398 \pm 0.070$	$-0.397^{+0.111}_{-0.083}$	$-0.436^{+0.126}_{-0.084}$
N6	$-0.399 \pm 0.095$	$-0.412^{+0.140}_{-0.103}$	$-0.445^{+0.154}_{-0.103}$


**Fig. 7.** Confidence contours (68.27%) and marginalized distributions for the parameters of the empirical relation fitted to the deep-field regions.

The parameters are consistent with those from DES-SN5YR and from Pantheon+ ( $z < 1.121$ ), as well as with those reported by Popovic et al. (2025) for the flat  $\Lambda$ CDM ( $\Omega_M = 0.330 \pm 0.015$ ),  $\Lambda$ CDM ( $\Omega_M = 0.279 \pm 0.057$ ,  $\Omega_k = 0.14 \pm 0.15$ ), and flat  $w$ CDM model ( $\Omega_M = 0.263^{+0.064}_{-0.078}$ ,  $w = -0.838^{+0.130}_{-0.142}$ ). The  $\Delta_{\text{AICc}}$  and  $\Delta_{\text{BIC}}$  values are similar to those for DES-SN5YR.

It is worth noting that the magnitude differences between a flat  $\Lambda$ CDM model with  $\Omega_M$  from Planck CMB measurements ( $\Omega_M^{\text{Planck}} = 0.3166$ ; Planck Collaboration et al. 2020) and the empirical relation have rms = 0.004 mag and a maximum absolute

deviation of  $\Delta m_{\text{max}} = 0.011$  mag, while the (rms,  $\Delta m_{\text{max}}$ ) values for the empirical relation calibrated with DES-SN5YR and Pantheon+ ( $z < 1.121$ ) are (0.012, 0.025) and (0.008, 0.014), respectively. Therefore, the empirical relation shows a close agreement with the flat  $\Lambda$ CDM model using  $\Omega_M^{\text{Planck}}$ , particularly when calibrated with DES-Dovekie and Pantheon+ ( $z < 1.121$ ).

The  $b$  values for the S1, S2, S4, and S5 regions in DES-Dovekie are  $-0.555 \pm 0.058$ ,  $-0.612 \pm 0.040$ ,  $-0.474 \pm 0.066$ , and  $-0.585 \pm 0.036$ , respectively. These values, together with those from S367, N147, N235, and N6, are mutually consistent within  $1.8\sigma$ . Using a LRT, we obtain  $\lambda = 6.6$  and a  $p$ -value of 0.36, indicating that the isotropic fit cannot be rejected. The  $b$  values from the S1, S2, S4, and S5 regions correspond to  $q_0$  values of  $-0.489 \pm 0.054$ ,  $-0.436 \pm 0.037$ ,  $-0.564 \pm 0.061$ , and  $-0.461 \pm 0.033$ , respectively.

We also constrain parameters using only DES SNe within DES-Dovekie. To do so, we select SNe with  $z > 0.093$ , which excludes the entire low- $z$  sample. We obtain  $b = -0.589 \pm 0.026$  for the empirical relation,  $\Omega_M = 0.307 \pm 0.020$  for the flat  $\Lambda$ CDM model, and  $q_0 = -0.488 \pm 0.029$  for the flat Padé model. The corresponding  $\Delta_{\text{IC}}$  values are 0.5, 0.0, and 2.1, indicating that the empirical relation and the flat  $\Lambda$ CDM model provide comparable fits to the Hubble diagram.

#### 4.7.2. Amalgame sample

The Amalgame sample (Popovic et al. 2024)<sup>4</sup> consists of 1792 photometrically classified SNe Ia from SDSS (Sako et al. 2011) and Pan-STARRS1 (Scolnic et al. 2018), with  $0.066 < z < 0.680$ . We obtain  $b = -0.613 \pm 0.041$  for the empirical relation,  $\Omega_M = 0.334^{+0.031}_{-0.027}$  for the flat  $\Lambda$ CDM model, and  $q_0 = -0.469^{+0.045}_{-0.041}$  for the flat Padé model. These values are consistent with those from Pantheon+ ( $z < 1.121$ ), DES-SN5YR, and DES-Dovekie. Fig. 8 shows the Hubble diagram for Amalgame.

<sup>4</sup> <https://github.com/bap37/AmalgameDR>

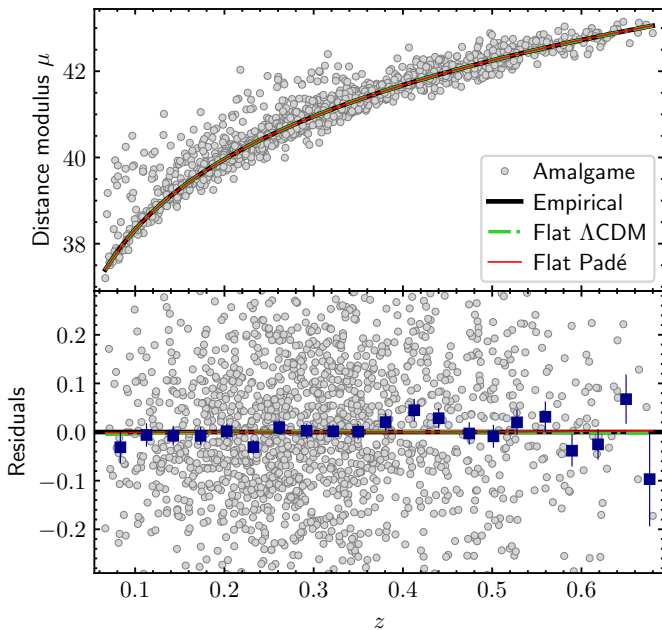


Fig. 8. Same as Fig. 4, but for the Amalgame SN sample.

The  $\Delta\text{IC}$  values for the empirical relation, the flat  $\Lambda\text{CDM}$  model, and the flat Padé model are 0.4, 0.0, and 0.6, respectively, indicating that they provide comparable fits to the Hubble diagram.

#### 4.7.3. BAO distances and cosmic chronometers

Although the empirical relation is designed to fit Hubble diagrams of standard candles, it is worth applying it to available  $d_M(z)$  and  $H(z)$  datasets. To do so, we assume the FLRW metric to transform the empirical relation into expressions for  $d_M(z)$  (Eq. 13) and  $H(z)$  (Eq. 14).

Abdul Karim et al. (2025) reported 13 distances measured from baryon acoustic oscillations (BAO) in DESI DR2, relative to the sound horizon  $r_d$ , at effective redshifts  $z_{\text{eff}}$  ranging from 0.295 to 2.33: six  $d_M(z)/r_d$  values, six  $d_H(z)/r_d$  values (with  $d_H(z) = c/H(z)$ ), and one  $d_V(z)/r_d$  value, where  $d_V(z) \equiv [z d_M(z)^2 d_H(z)]^{1/3}$ .<sup>5</sup> Fitting Eqs. (13) and (14) to the seven BAO distances with  $z_{\text{eff}} < 1.121$ , and assuming  $\Omega_k = 0$ , we obtain  $b = -0.584 \pm 0.016$ . For comparison, the  $b$  values obtained from Pantheon+ ( $z < 1.121$ ), DES-SN5YR, DES-Dovekie, and Amalgame, when all SN samples are restricted to  $z \geq 0.295$ , are  $-0.697 \pm 0.050$ ,  $-0.622 \pm 0.035$ ,  $-0.618 \pm 0.033$ , and  $-0.688 \pm 0.070$ , respectively. Compared to the BAO constraint, the latter three values are consistent within  $1.4\sigma$ , while the Pantheon+ ( $z < 1.121$ ) result is marginally consistent, showing a  $2.2\sigma$  difference.

Alfano et al. (2026) collected 34  $H(z)$  values measured with cosmic chronometers, with  $0.07 \leq z \leq 1.965$ . Fitting Eq. (14) to the 27  $H(z)$  values with  $z < 1.121$ , and assuming  $\Omega_k = 0$ , we obtain  $b = -0.635 \pm 0.095$ . This value is consistent with those from Pantheon+ ( $z < 1.121$ ), DES-SN5YR, DES-Dovekie, and Amalgame when all SN samples are restricted to  $z \geq 0.07$ , yielding  $b = -0.617 \pm 0.033$ ,  $-0.607 \pm 0.027$ ,  $-0.591 \pm 0.024$ , and  $-0.613 \pm 0.041$ , respectively.

<sup>5</sup> Data are available at [https://github.com/CobayaSampler/bao\\_data/tree/master/desi\\_bao\\_dr2](https://github.com/CobayaSampler/bao_data/tree/master/desi_bao_dr2)

Table 8. Values of  $\hat{j}_0$  for different magnitude–redshift relations

Relation	Pantheon+ ( $z < 1.121$ )	DES-SN5YR
	$\hat{j}_0$	$\hat{j}_0$
Empirical	$0.585^{+0.014}_{-0.011}$	$0.596^{+0.012}_{-0.011}$
$\Lambda\text{CDM}$	$0.902^{+0.371}_{-0.415}$	$0.726^{+0.298}_{-0.339}$
Flat $w\text{CDM}$	$0.909^{+0.672}_{-0.575}$	$0.514^{+0.409}_{-0.345}$
Padé	$1.323^{+1.324}_{-0.660}$	$0.664^{+0.851}_{-0.452}$

## 5. Discussion

### 5.1. Jerk parameter

The value of  $j_0$  provides an observational test for the flat  $\Lambda\text{CDM}$  model (Bochner et al. 2015). Indeed, for the non-flat  $w\text{CDM}$  model (Eq. 4), Eq. (6) yields  $j_0 = 1 - \Omega_k + 3(1+w)(2q_0 + \Omega_k - 1)/2$ , which reduces to  $j_0 = 1$  for the flat  $\Lambda\text{CDM}$  model. Therefore, if  $j_0$  deviates from unity, it could indicate that the Universe is not flat, dark energy is not a cosmological constant, or that Eq. (4) is incorrect. Given that  $\hat{j}_0 = 1$  for the flat  $\Lambda\text{CDM}$  model, the test remains valid if  $\hat{j}_0$  is used instead of  $j_0$ .

Table 8 lists the  $\hat{j}_0$  values. For the empirical relation we use

$$\hat{j}_0 = \frac{9}{4} \left( \frac{5}{9} + q_0 \right)^2 + \frac{5}{9}, \quad (16)$$

which is derived from Eqs. (6) and (14). For DES-SN5YR and Pantheon+ ( $z < 1.121$ ), the  $\hat{j}_0$  values are consistent within  $1.2\sigma$ . In particular, the  $\hat{j}_0$  values for the  $\Lambda\text{CDM}$  model, the flat  $w\text{CDM}$  model, and the Padé cosmography are consistent with unity within  $1.2\sigma$ . In contrast, the  $\hat{j}_0$  values for the empirical relation are approximately 0.4 below unity, with an overwhelming significance of at least  $30\sigma$ . Assuming  $w = -1$ , these values translate to  $\Omega_k = 0.208^{+0.005}_{-0.007}$  and  $0.202^{+0.005}_{-0.006}$  for Pantheon+ ( $z < 1.121$ ) and DES-SN5YR, respectively; or, assuming  $\Omega_k = 0$ , to  $w = -0.853 \pm 0.001$  and  $-0.854 \pm 0.001$ , respectively. Note, however, that the empirical relation is intended to fit the Hubble diagram, not its derivatives. Therefore, although the empirical relation provides  $q_0$  values consistent with those from other  $m(z)$  relations (see Table 4), it may misestimate  $\hat{j}_0$ .

### 5.2. Cosmic anisotropies through hemisphere comparison

Pantheon+ has been widely used to search for anisotropies in cosmological parameters using the hemisphere comparison (HC) method (Schwarz & Weinhorst 2007) under different cosmological models (e.g., Mc Conville & Ó Colgáin 2023; Clocchiatti et al. 2024; Hu et al. 2024b,a). The HC method splits the sky into two opposite hemispheres (‘up’ and ‘down’), constrains the cosmological parameter  $x$  in each, computes a statistic such as the signal-to-noise ratio (S/N) of  $\Delta x = |x_{\text{up}} - x_{\text{down}}|$ , and repeats the procedure for different directions across the sky.

We apply the HC method to Pantheon+ ( $z < 1.121$ ) using the empirical relation. We select a set of directions on the celestial sphere using HEALPY (Górski et al. 2005; Zonca et al. 2019) with a grid resolution parameter  $N_{\text{side}} = 128$ . This provides 196.608 equal-area pixels on the sky, corresponding to a set of 98.304 independent directions. For each direction, we compute  $S/N(\Delta x) = \Delta x / (\sigma_{\text{up}}^2 + \sigma_{\text{down}}^2 - 2\sigma_{\text{up,down}})^{1/2}$ , where  $\sigma_{\text{up}}$  and  $\sigma_{\text{down}}$  are the uncertainties of  $x_{\text{up}}$  and  $x_{\text{down}}$ , respectively, and  $\sigma_{\text{up,down}}$  is their covariance. Fig. 9 shows the sky maps of  $S/N(\Delta M)$  and  $S/N(\Delta b)$ . Their maximum values are 3.7 at (RA, Dec)=(239.2°, -70.17°) and 3.3 at (RA, Dec)=(212.3°, -39.07°), respectively.

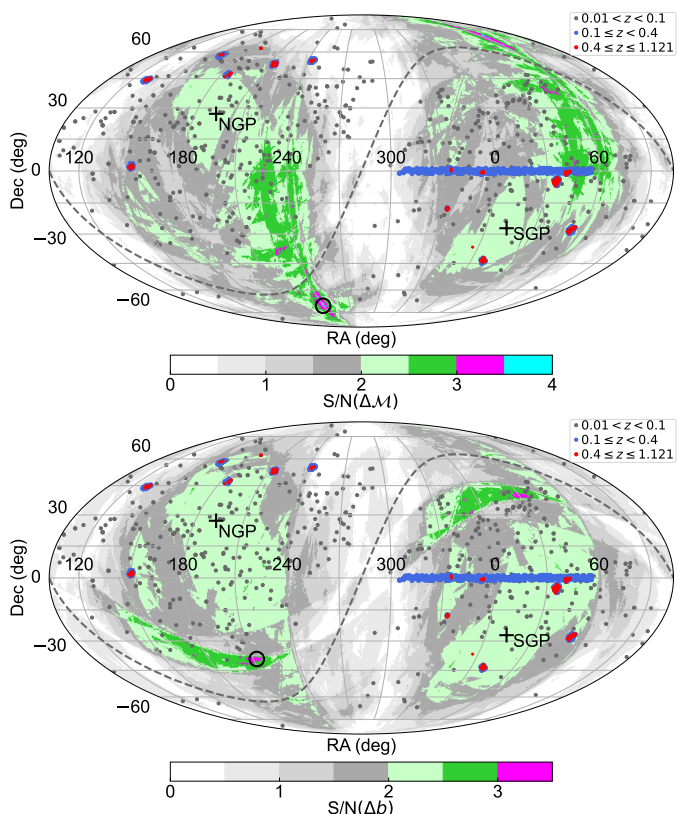


**Fig. 9.** Sky maps of  $S/N(\Delta M)$  and  $S/N(\Delta b)$ . Dots represent the SNe in Pantheon+ ( $z < 1.121$ ) and circles mark the maximum  $S/N$  values.

To evaluate the probabilities of obtaining  $S/N(\Delta M) \geq 3.7$  and  $S/N(\Delta b) \geq 3.3$  by chance when scanning many directions on the sky (the look-elsewhere effect; Bayer & Seljak 2020), we perform  $10^4$  simulations. In each simulation, we randomize the RA and Dec coordinates of the SNe and produce the  $S/N(\Delta M)$  and  $S/N(\Delta b)$  maps with the HC method and the same directions used above. The probabilities of obtaining  $S/N(\Delta M) \geq 3.7$  and  $S/N(\Delta b) \geq 3.3$  by chance are 6.0% and 11.2%, respectively, corresponding to significances of  $1.9\sigma$  and  $1.6\sigma$ . Therefore, we find no evidence for anisotropies in  $M$  and  $b$ .

If the directions of maximum  $S/N(\Delta M)$  and  $S/N(\Delta b)$  were real anisotropies, detecting them at a  $3\sigma$  level with the HC method would require adding 2500 and 4400 SNe to Pantheon+ ( $z < 1.121$ ), respectively. Another alternative would be to perform deep-field SN surveys toward the directions of the candidate anisotropies. This is particularly important given the absence of high- $z$  SNe near those directions (see Fig. 9).

### 5.3. JWST, LSST, CSST, and Roman

Given the small number of SNe at  $z > 1.121$ , the validity of the empirical relation beyond this redshift remains to be verified. Currently, the James Webb Space Telescope (JWST) is observing SNe Ia at  $z > 1.7$  (Casey et al. 2023; DeCoursey et al. 2025). Siebert et al. (2025) reported  $\mu = 46.08^{+0.19}_{-0.18}$  for SN 2025ogs at  $z = 2.05$ , while Pierel et al. (2025) reported  $\mu = 46.10^{+0.17}_{-0.18}$  for SN 2023aeax at  $z = 2.15$  and  $\mu = 47.14^{+0.21}_{-0.24}$  for SN 2023adsy at  $z = 2.903$ . At these redshifts, using the parameters inferred from Pantheon+ (Table 2) and  $H_0 = 70 \text{ km s}^{-1} \text{ Mpc}^{-1}$ , the predictions of the empirical relation are  $\mu = 45.92, 46.04,$  and  $46.71$ , respectively, while those of the  $\Lambda$ CDM model are  $\mu = 46.0, 46.13,$  and

46.94, respectively. The  $\mu$  values for SN 2025ogs and 2023aeax are consistent with both relations, whereas that for SN 2023adsy is more consistent with the  $\Lambda$ CDM model than with the empirical relation. However, due to its red color, it is still unclear whether SN 2023adsy is representative of high- $z$  SNe Ia or an outlier (Pierel et al. 2024, 2025).

In addition to JWST, the deep-field surveys of the future China Space Station Telescope (CSST; Li et al. 2023) and the Nancy Grace Roman Space Telescope (Hounsell et al. 2023) will observe SNe Ia up to  $z = 1.3$  and  $z = 1.7$ , respectively. These SNe, together with those observed by JWST and the 19 SNe at  $1.121 < z \leq 2.261$  in Pantheon+, will be crucial for determining the highest  $z$  at which the empirical relation remains valid.

The deep rolling surveys of the Vera C. Rubin Observatory Legacy Survey of Space and Time (LSST; Gris et al. 2024) will provide photometry of thousands of SNe Ia with  $z \leq 1.1$ . Therefore, the Hubble diagram for each of the five LSST Deep Drilling Fields can be analyzed with the empirical relation. Of these fields, the newly defined Euclid Deep Field South (RA=61.241°, Dec=−48.423°), located at an angular separation of 21° from the S5 field, will allow us to study cosmic acceleration in a different direction from those analyzed in this work.

## 6. Conclusions

We have presented a new empirical  $m(z)$  relation based on data from Pantheon+ and DES-SN5YR. This relation fits their Hubble diagrams with only two parameters,  $M$  and  $b$ , both of which can be computed analytically. In particular, under the FLRW metric,  $b \propto q_0 + 1$ .

For the DES-SN5YR and Pantheon+ Hubble diagrams, the empirical relation provides fits up to  $z = 1.121$  that closely match those obtained with the Padé cosmography and the  $\Lambda$ CDM, flat  $\Lambda$ CDM, flat  $w$ CDM, and flat Padé models. The validity of the empirical relation beyond  $z = 1.121$  cannot be reliably assessed given the small number of SNe at  $z > 1.121$ . Based on the  $\Delta_{IC}$  values, the empirical relation performs better than the  $\Lambda$ CDM model, the flat  $w$ CDM model, and the Padé cosmography, and comparably to the flat  $\Lambda$ CDM and flat Padé models.

For DES-SN5YR and Pantheon+ ( $z < 1.121$ ), we obtain  $b = -0.628 \pm 0.021$  and  $b = -0.606 \pm 0.026$ , respectively. We also applied the empirical relation to DES-Dovekie and Amalgame, obtaining  $b = -0.603 \pm 0.020$  and  $b = -0.613 \pm 0.041$ , respectively. For Pantheon+ ( $z < 1.121$ ) combined with SHOES, we obtain  $H_0 = 73.4 \pm 1.0 \text{ km s}^{-1} \text{ Mpc}^{-1}$ .

The empirical relation, as well as the flat  $\Lambda$ CDM and the flat Padé models, is relatively stable in the absence of low- $z$  SNe. We fit the empirical relation to the Hubble diagrams of the eight deep-field regions, finding that their fitted  $M$  and  $b$  parameters are consistent within  $1.6\sigma$ , in agreement with isotropy. Applying a LRT, we find no evidence of anisotropy. The latter is further supported by using the empirical relation in the HC method applied to Pantheon+ ( $z < 1.121$ ), which finds no statistically significant evidence for anisotropies in  $M$  and  $b$ .

Furthermore, the  $b$  values from the eight deep-field regions translate to  $q_0$  values ranging from  $-0.6$  to  $-0.4$ , which are consistent within  $1.6\sigma$  and lower than zero at  $4.8\sigma$ . These results strongly support an accelerating universe, under the assumption that the large-scale density in each deep-field region is independent of the comoving radial coordinate.

Under the assumption of the FLRW metric, the empirical relation can also be applied to BAO distances from DESI DR2, and  $H(z)$  values from cosmic chronometers. The derived  $b$  values,

assuming  $\Omega_k = 0$ , are mostly consistent with those from DES-SN5YR, Pantheon+ ( $z < 1.121$ ), DES-Dovekie, and Amalgame.

The empirical relation  $m(z) = \mathcal{M} + bz + 5 \log(z(1+z))$ , or equivalently  $d_L(z) = \frac{cz}{H_0}(1+z)10^{bz/5}$ , provides a straightforward quantitative tool for fitting Hubble diagrams of SNe Ia without the need to add a low- $z$  sample. It enables tests of basic properties of the Universe in a simplified manner, reducing the computational cost typically associated with physically motivated cosmological models. Our analysis shows that the empirical relation is valid up to at least  $z \approx 1.1$ . Ongoing and upcoming deep SN surveys will allow us to test whether it holds at higher redshifts.

*Acknowledgements.* We acknowledge the Director of the Millennium Institute of Astrophysics (MAS), Francisco Förster, for financial assistance through ANID grant ICN12\_009, and acknowledge complementary funding from ANID/FONDECYT grant 1251692. OR is supported by the Rubin-Chile Fund under grant DIA2650. We thank Felipe Asenjo and Ariel Órdenes for helpful discussions.

## References

- Abdul Karim, M., Aguilar, J., Ahlen, S., et al. 2025, *Phys. Rev. D*, 112, 083515
- Alfano, A. C., Cafaro, C., Capozziello, S., Luongo, O., & Muccino, M. 2026, *Journal of High Energy Astrophysics*, 49, 100444
- Baker, G. A. & Graves-Morris, P. 1996, *Pade approximants* (Cambridge, UK: Cambridge University Press)
- Bayer, A. E. & Seljak, U. 2020, *J. Cosmology Astropart. Phys.*, 2020, 009
- Bochner, B., Pappas, D., & Dong, M. 2015, *ApJ*, 814, 7
- Brout, D., Scolnic, D., Popovic, B., et al. 2022, *ApJ*, 938, 110
- Burnham, K. P. & Anderson, D. R. 2002, *Model selection and multimodel inference: a practical information-theoretic approach* (New York: Springer-Verlag)
- Camilleri, R., Davis, T. M., Vincenzi, M., et al. 2024, *MNRAS*, 533, 2615
- Capozziello, S., D’Agostino, R., & Luongo, O. 2020, *MNRAS*, 494, 2576
- Casey, C. M., Kartaltepe, J. S., Drakos, N. E., et al. 2023, *ApJ*, 954, 31
- Cattoën, C. & Visser, M. 2007, *Classical and Quantum Gravity*, 24, 5985
- Clocchiatti, A., Rodríguez, Ó., Órdenes Morales, A., & Cuevas-Tapia, B. 2024, *ApJ*, 971, 19
- Conley, A., Guy, J., Sullivan, M., et al. 2011, *ApJS*, 192, 1
- DeCoursey, C., Egami, E., Pierel, J. D. R., et al. 2025, *ApJ*, 979, 250
- Earp, S. W. F., Debatista, V. P., Macciò, A. V., et al. 2019, *MNRAS*, 488, 5728
- Efstathiou, G. 2025, *Philosophical Transactions of the Royal Society of London Series A*, 383, 20240022
- Enqvist, K. 2008, *General Relativity and Gravitation*, 40, 451
- Foreman-Mackey, D., Hogg, D. W., Lang, D., & Goodman, J. 2013, *PASP*, 125, 306
- Gelman, A. & Rubin, D. B. 1992, *Statistical Science*, 7, 457
- Górski, K. M., Hivon, E., Banday, A. J., et al. 2005, *ApJ*, 622, 759
- Gris, P., Awan, H., Becker, M. R., et al. 2024, *ApJS*, 275, 21
- Hounsell, R., Scolnic, D., Brout, D., et al. 2023, *arXiv e-prints*, arXiv:2307.02670
- Hu, J. P., Hu, J., Jia, X. D., Gao, B. Q., & Wang, F. Y. 2024a, *A&A*, 689, A215
- Hu, J. P. & Wang, F. Y. 2022, *A&A*, 661, A71
- Hu, J. P., Wang, Y. Y., Hu, J., & Wang, F. Y. 2024b, *A&A*, 681, A88
- Huang, L., Cai, R.-G., & Wang, S.-J. 2025, *Science China Physics, Mechanics, and Astronomy*, 68, 100413
- Kass, R. E. & Raftery, A. E. 1995, *Journal of the American Statistical Association*, 90, 773
- Koyama, K. 2016, *Reports on Progress in Physics*, 79, 046902
- Li, E.-K., Du, M., & Xu, L. 2020, *MNRAS*, 491, 4960
- Li, S.-Y., Li, Y.-L., Zhang, T., et al. 2023, *Science China Physics, Mechanics, and Astronomy*, 66, 229511
- Linder, E. V. 2006, *Phys. Rev. D*, 74, 103518
- Mc Conville, R. & Ó Colgáin, E. 2023, *Phys. Rev. D*, 108, 123533
- Odintsov, S. D., Sáez-Chillón Gómez, D., & Sharov, G. S. 2025, *European Physical Journal C*, 85, 298
- Perivolaropoulos, L. & Skara, F. 2022, *New A Rev.*, 95, 101659
- Perlmutter, S., Aldering, G., Goldhaber, G., et al. 1999, *ApJ*, 517, 565
- Pierel, J. D. R., Coulter, D. A., Siebert, M. R., et al. 2025, *ApJ*, 981, L9
- Pierel, J. D. R., Engesser, M., Coulter, D. A., et al. 2024, *ApJ*, 971, L32
- Planck Collaboration, Aghanim, N., Akrami, Y., et al. 2020, *A&A*, 641, A6
- Popovic, B., Scolnic, D., Vincenzi, M., et al. 2024, *MNRAS*, 529, 2100
- Popovic, B., Shah, P., Kenworthy, W. D., et al. 2025, *arXiv e-prints*, arXiv:2511.07517
- Räsänen, S. 2006, *J. Cosmology Astropart. Phys.*, 2006, 003
- Riess, A. G., Filippenko, A. V., Challis, P., et al. 1998, *AJ*, 116, 1009
- Riess, A. G., Yuan, W., Macri, L. M., et al. 2022, *ApJ*, 934, L7
- Sako, M., Bassett, B., Connolly, B., et al. 2011, *ApJ*, 738, 162
- Sánchez, B. O., Brout, D., Vincenzi, M., et al. 2024, *ApJ*, 975, 5
- Schwarz, D. J. & Weinhorst, B. 2007, *A&A*, 474, 717
- Schwarz, G. 1978, *Annals of Statistics*, 6, 461
- Scolnic, D. M., Jones, D. O., Rest, A., et al. 2018, *ApJ*, 859, 101
- Siebert, M. R., Pierel, J. D. R., Engesser, M., et al. 2025, *arXiv e-prints*, arXiv:2512.19783
- Sugiura, N. 1978, *Commun. Stat. Theory Methods*, 7, 13
- Vincenzi, M., Kessler, R., Shah, P., et al. 2025, *MNRAS*, 541, 2585
- Weinberg, D. H., Mortonson, M. J., Eisenstein, D. J., et al. 2013, *Phys. Rep.*, 530, 87
- Wilks, S. S. 1938, *Annals of Mathematical Statistics*, 9, 60
- Wiltshire, D. L. 2009, *Phys. Rev. D*, 80, 123512
- Zonca, A., Singer, L., Lenz, D., et al. 2019, *The Journal of Open Source Software*, 4, 1298